RSC Advances

PAPER

View Article Online
View Journal | View Issue

Cite this: *RSC Adv.*, 2017, **7**, 26704

Synthesis, characterization and application of TiO_2/Ag recyclable SERS substrates†

Qingli Huang,[ac] Jing Li,[b] Wenxian Wei,[c] Yongping Wu *[a] and Ting Li*[a]

Received 16th March 2017
Accepted 14th May 2017

DOI: 10.1039/c7ra03112b

rsc.li/rsc-advances

In this paper, rutile and anatase TiO_2/Ag nanocomposites were prepared by a facile and green photochemical method. The as-prepared samples were investigated by using various spectroscopic and microscopic techniques in detail. Trace detection of rhodamine 6G (R6G) and crystal violet (CV) was studied based on the nanocomposites. Compared to the anatase TiO_2/Ag nanocomposite, the rutile TiO_2/Ag nanocomposites (S_{r3}) exhibited the best SERS performance for rhodamine 6G (R6G). Then, the optimized SERS-active substrates (S_{r3}) were employed to study its recycling properties by degrading R6G and CV *in situ*. The substrates were able to self-clean. The possible mechanism of the good SERS and photocatalytic performance of the TiO_2/Ag nanocomposite (S_{r3}) was discussed. This work is of importance in theoretical research and practical application based on the SERS effect of nanocomposites.

1. Introduction

With wide use of dyes, effective detection and removal of organic pollutants from the environment has been a pressing issue, because many organic dyes are quite stable and toxic. A variety of techniques have been developed to detect and remove organic dyes from the environment. Surface-enhanced Raman spectroscopy (SERS) is thought to be a promising technique for the trace detection and analysis of organic dyes in the environment due to its good sensitivity and exceptional spectral selectivity.[1–5] The SERS effect is a phenomenon where the Raman signal intensity of molecules can be dramatically enhanced when the molecules are adsorbed on (or close to) the metal material surface. Since the first observation of SERS on a rough silver electrode in 1974, SERS has attracted much attention due to its high sensitivity, speed of detection and fingerprint features. In the last decades, various noble metals nanomaterials were prepared as typical SERS-active substrates.[6–9] However, as SERS substrates, the traditional noble metal materials are for one-time use only and cannot remove the pollutants, which limits the development of SERS substrates. Photocatalysis has been proven to be an effective method to degrade organic dyes into simpler and harmless compounds to eliminate environmental pollution.[10–13] In the past decades, considerable efforts have been made toward the development of novel multifunctional nanomaterials which possessed both high surface enhanced Raman scattering (SERS) activity and enhanced photocatalytic activity.[14–21] However, most methods need a long time or complicated instrumentation, therefore it is necessary to develop new time-saving and cost-effective methods to prepare these nanomaterials.

Semiconductor nanomaterials have been extensively studied from both theoretical and experimental points due to their high photocatalytic performance.[22–24] Of the well-known semiconductor nanomaterials, titanium oxide (TiO_2) nanoparticle has been proved to be a suitable photocatalyst owing to its unique and superior properties, such as cheap, easy acceptance, non-toxicity, photo-stability, and so on.[22–27] However, the main drawbacks of low quantum yields and the lack of visible light utilization constrain the practical usage of TiO_2. Efforts have been made to improve the photocatalytic activity of TiO_2 by various methods. One of the methods for improving photocatalyst performance is addition of nanoparticles of noble metals deposited on TiO_2 surface.[28–35] Various noble metal nanoparticles/TiO_2 composites have been prepared by many methods.[28–35] Compared with other deposition techniques, photoreduction has the advantages of environment protection, energy saving and high reproducibility.

The advantage of plasma noble metals and photocatalytic semiconductor nanomaterials of noble metal nanoparticles/TiO_2 composites offer an opportunity to detect and remove the adsorbed molecules *in situ* on a single material.[36–49] Herein, rutile and anatase TiO_2/Ag nanocomposites were prepared by a facile and green photochemical method. The as-synthesized nanocomposites were characterized using X-ray diffraction (XRD), transmission electron microscope (TEM), X-ray photoelectron spectroscopy (XPS), UV-vis absorption spectroscopy (UV-vis), X-ray fluorescence spectrometer (XRF), Zahner

[a]*Research Facility Center for Morphology of Xuzhou Medical University, Xuzhou City, Jiangsu 221004, China. E-mail: 100002016057@xzhmu.edu.cn; wyp@xzhmu.edu.cn; Fax: +86-516-83262091*

[b]*School of Chemistry and Chemical Engineering, Xuzhou Institute of Technology, Xuzhou City, Jiangsu, 221111, China*

[c]*Testing Center, Yangzhou University, Yangzhou City, Jiangsu 225009, China*

† Electronic supplementary information (ESI) available. See DOI: 10.1039/c7ra03112b

workstation and Raman spectrometer (Raman). The surface-enhanced Raman scattering (SERS) performance and photocatalytic activity of the nanocomposites were also investigated. It can be found that rutile TiO_2/Ag nanocomposites (S_{r3}) have good SERS and photocatalytic performances, which will be used as novel SERS substrates for detection and elimination *in situ* of organic pollutants on a single substrate. The synthesis process is straightforward, simple, reproducible, cost effective and robust. In the future, the present process may be helpful for the synthesis of other types of nanomaterials in a small time scale with higher yields.

2. Experimental section

2.1. Material

All the chemical reagents used in this work, including anatase titanium oxide (TiO_2), rutile titanium oxide (TiO_2), silver nitrate ($AgNO_3$), rhodamine 6G (R6G), crystal violet (CV) was purchase from Sigma-Aldrich Chemical Co., Ltd. (Shanghai, China). All chemicals were of analytical grade. Deionized water was used throughout the experiment.

2.2. Methods

Synthesis of TiO_2/Ag nanocomposites: firstly, 3 mmol (0.72 g) rutile titanium oxide were dispersed in 100 mL deionized water with vigorous stirring. Then a certain amount of silver nitrate (0.5 mmol, 1 mmol and 3 mmol) was added into the above suspension, respectively. Finally, the mixed solution was irradiated under a 250 W UV lamp for 120 min. The obtained products were collected by centrifugation and washed with deionized water and ethanol for several times. The final products were dried at 70 °C for 10 h and denoted as Sr_1, S_{r2} and S_{r3}. Similar procedure of was performed under the same reaction condition except using anatase titanium oxide instead of rutile titanium oxide and the resulting products were denoted as Sa_1, S_{a2} and S_{a3}.

2.3. Characterization

The phase purity of the products was characterized by X-ray diffraction (XRD, German Bruker AXSD8 ADVANCE X-ray diffractometer) using a X-ray diffractometer with Cu KR radiation ($\lambda = 1.5418$ Å). Transmission electron microscope (TEM) images and elemental mapping images were obtained on an American FEI Tecnai G2 F30 S-TWIN field-emission transmission electron microscopy (operated at 300 kV). The ultraviolet-visible (UV-vis) diffuse reflectance spectra were obtained on an America Varian Cary 5000 spectrophotometer. X-ray photoelectron spectra (XPS) were recorded on an ESCALAB 250Xi system (Thermo Scientific). Prior to the analysis in the XPS system, all investigated materials, in the form of powder, were pasted onto the surface of the sample stage. All XPS measurements were performed using the ESCALAB 250Xi system without external illumination. A monochromated Al Kα X-ray source (1486.6 eV) was used and operated at a voltage of 15 kV. The chosen pass energy was found to provide a reasonable compromise between the energy resolution and transmission of the analyzer, in other words good quality spectra with a satisfactory signal to noise ratio could be recorded within acceptably short acquisition times. In order to neutralize the charge build-up on the investigated surfaces, the XPS tool is equipped with a standard dual flood gun, which provides simultaneously a beam of low energy electrons and a beam of low energy Ar-ions. XPS spectra were carried out with the binding energies calibrated using C 1s (284.8 eV). The SERS and self-cleaning process were preformed on the glass where the dyes and the as-prepared samples were mixed. For SERS spectral examination, 1 mL R6G aqueous solution was dispersed on the samples at different concentrations and dried in the air. SERS spectra were measured by using a Raman spectrometer (Britain Renishaw Invia Raman spectrometer) with a 532 nm Ar ion laser line, where the effective power of the laser source was 0.35 mW. Spectra were accumulated 1 scans. The total accumulation time for SERS and Raman measurements was 10 s. The beam diameter was approximately 2 μm on the sample surface. The self-cleaning process was preformed on the above glass under the irradiation by an 1000 W Xe lamp for 1 h.

3. Results and discussion

Fig. 1 shows the TEM images of the TiO_2/Ag nanocomposites prepared with different amount of $AgNO_3$. It can be found that there are many dense dark dots with a size range of 1–3 nm on the surface of TiO_2 nanoparticles. Moreover, the distribution densities of the dots on the surfaces of TiO_2 nanoparticles (NPs) gradually increased when the amount of $AgNO_3$ in the precursor suspensions were increased form 0.085 g to 0.51 g (Fig. 1a–c). To further characterize the as-prepared samples, the STEM and EDS mapping images were also obtained on an American FEI Tecnai G2 F30 S-TWIN field-emission transmission electron microscopy, which is shown in Fig. 1d. Different colors indicate different elements: yellow, red and blue refer to the presence of Ti, O and Ag respectively. Obviously, the TiO_2/Ag nanocomposites were prepared by a simple photochemical method and Ag nanoparticles were decorated uniformly on the TiO_2.

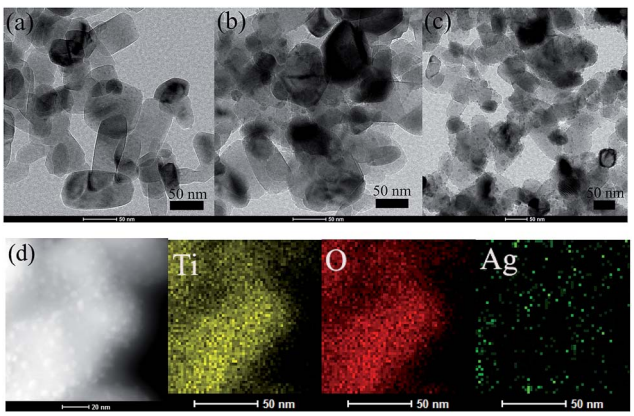

Fig. 1 TEM images of the TiO_2/Ag nanocomposites were prepared using different amount of $AgNO_3$ (a) 0.085 g (S_{r1}) (b) 0.17 g (S_{r2}) (c) 0.51 g (S_{r3}) and EDS mapping images (d) S_{r3}.

Fig. 2 shows a typical XRD pattern of the as-prepared TiO_2/Ag nanocomposites (S_{r1}, S_{r2} and S_{r3}). Two sets of diffraction patterns are found in Fig. 2: those diffraction peaks marked with "#" are indexed to rutile TiO_2 (JCPDS 21-1276), while the peak marked with "*" are ascribed to face-centered cubic (fcc) metallic Ag (JCPDS 04-0783). The intensity of major reflections of TiO_2 became weak with the increase of the amounts of $AgNO_3$ in the precursor suspensions. Comparatively, the peak of Ag marked with "*" became strong with the increase of the amounts of $AgNO_3$ in the precursor suspensions. This phenomenon indicates that the TiO_2/Ag nanocomposites synthesized using a higher [Ag^+] precursor solution contain larger amount of metal Ag nanoparticles, which is well agree with the results of TEM.

The diffuse reflectance spectra of the as-prepared samples were demonstrated in Fig. 3. The absorption edge at about 400 nm is assigned to the absorption of TiO_2 semiconductor in Fig. 3a. For the TiO_2/Ag nanocomposites shown in Fig. 3b–d, broad absorptions of 400–800 nm were found, which should be due to the localized surface-plasmon-resonance (LSPR) effect of Ag nanoparticles on the surfaces of the TiO_2. It can be seen that the intensities of visible-light absorption peaks of TiO_2/Ag nanocomposites increased with the amount of Ag nanoparticles on the surface of TiO_2. However, the maximum visible-light absorption peaks of TiO_2/Ag nanocomposites are similar both in location and in shape, which may be attributed to the same shapes and sizes of Ag nanoparticles on the surface of TiO_2. This point can be confirmed by the TEM observations.

To elucidate the chemical state of elements in Ag/TiO_2 composite, XPS analysis was performed. Fig. 4a clearly indicates that the major sets of peaks from the O 1s, Ti 2p and Ag 3d states exist in the Ag/TiO_2. No trace of any impurity is observed, except for a small amount of adventitious carbon (C 1s) from the XPS instrument itself (Fig. 4b). The high-resolution Ti 2p curve (Fig. 4c) demonstrates two peaks at 459.1 and 464.8 eV, which belong to the Ti $2p_{3/2}$ and Ti $2p_{1/2}$ orbits, respectively, indicating the presence of Ti^{4+}.[50] The characteristic doublet peaks for Ag in Fig. 4d were also observed at binding energies of 368.1 eV and 374.1 eV for Ag $3d_{5/2}$ and Ag $3d_{3/2}$ respectively, with a separation of 6 eV, confirming the presence of zero valent Ag in Ag/TiO_2 composites. The XPS results further demonstrated that Ag nanoparticles have been loaded in the TiO_2.

To obtain the SERS substrates with best performance, the SERS spectra of R6G (1×10^{-5} M) were obtained on different TiO_2/Ag nanocomposites. Fig. 5a–c show the SERS spectra of different TiO_2/Ag nanocomposites prepared with different amount of $AgNO_3$ using R6G (1×10^{-5} M) as model Raman probes. The peaks from 400 to 2000 cm^{-1} were attributed to R6G signals. The peaks at about 612 and 769 cm^{-1} are assigned to an in-plane bending mode of the C–C–C ring and an out-of-plane bending motion of C–H of the xanthene skeleton, respectively. The peaks at 1364, 1507, and 1651 cm^{-1} are ascribed to the C–C stretching modes. The sample S_{r3} displayed the strongest SERS signal intensity, which decreased with decreasing amount of the Ag nanoparticles on the surface of TiO_2 (Fig. 5, curve a–c). To further investigate the SERS performance of S_{r3}, the SERS spectra of anatase TiO_2/Ag nanocomposites (S_{a3}) were also investigated. It can be found that the signal intensity of R6G (1×10^{-5} M) absorbed on the S_{a3} became very weak in Fig. 5, curve d. As we all know, the SERS effect of SERS substrates on the absorbed probe molecules depends on the size and density of noble metal nanoparticles. Compared to rutile TiO_2/Ag (S_{r3}) nanocomposites, there are relative sparse Ag nanoparticles on the surface of anatase TiO_2/Ag nanocomposites (Fig. S1†). XRF results further confirmed the case (Table 1). It is clear that the appropriate size and

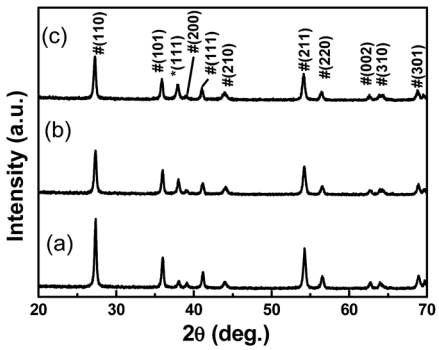

Fig. 2 XRD patterns of the TiO_2/Ag nanocomposites prepared with different amount of $AgNO_3$ (a) Sr_1 (b) Sr_2 (c) Sr_3.

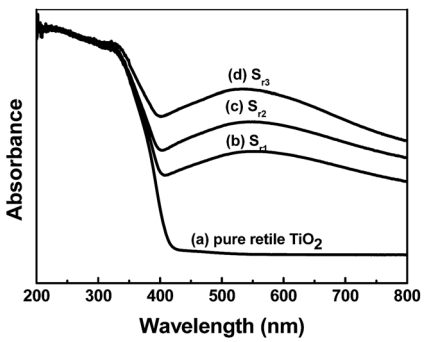

Fig. 3 DRS spectra of the pure rutile TiO_2 and rutile TiO_2/Ag nanocomposites.

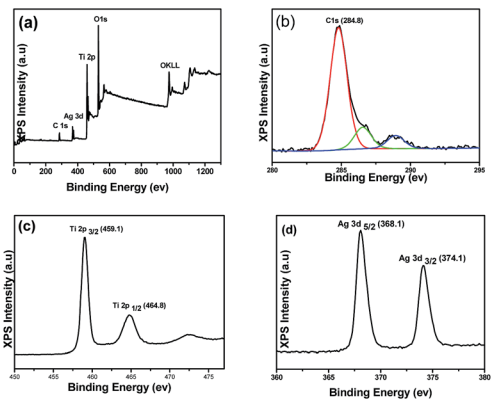

Fig. 4 (a) XPS spectra of rutile TiO_2/Ag nanocomposites (S_{r3}) and (b–d) high resolution XPS spectrum of C, Ti and Ag elements respectively.

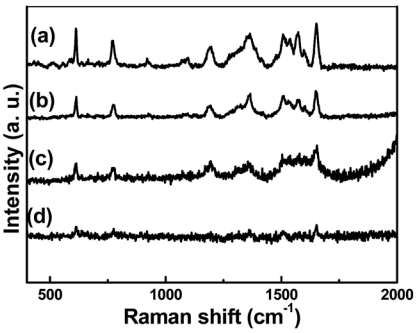

Fig. 5 The SERS spectra of R6G (1×10^{-5} M) were obtained on different TiO_2/Ag nanocomposites (a) S_{r1} (b) S_{r2} (c) S_{r3} (d) S_{a3}.

Table 1 The weight percentage Ag of the as-prepared samples was obtained by XRF

Sample	S_{r1}	S_{r2}	S_{r3}	S_{a1}	S_{a2}	S_{a3}
Weight percentage of Ag	2.20%	4.63%	6.05%	0.62%	1.11%	2.23%

density of Ag nanoparticles in S_{r3} is suitable for the generation of Raman "hot spots".

The reproducibility of the substrate is an important factor for SERS detection. The reproducibility of SERS performance of TiO_2/Ag nanocomposites (S_{r3}) was also investigated. Five spots in the TiO_2/Ag nanocomposites (S_{r3}) substrate were randomly chosen to analyze the stability of Raman spectrum detection. Fig. 6 shows the SERS spectra of R6G (1×10^{-5} M) were obtained on different spots of TiO_2/Ag nanocomposites. As shown in Fig. 6a, the Raman spectra taken at different positions are nearly same. The intensity of the peaks at 1651 cm^{-1} and 769 cm^{-1} were chosen as parameters to character the reproducibility of the SERS enhancement as provided in Fig. 6b. The deviations of signal intensities were calculated 9.28% at 1651 cm^{-1} and 12.8% at 769 cm^{-1}, respectively. The small dispersion of detection signals within 20% confirmed the advantages of the TiO_2/Ag nanocomposites (S_{r3}) as reliable and reproducible SERS substrates.

Fig. 7a shows the SERS spectra using TiO_2/Ag nanocomposites substrate (S_{r3}) for different concentrations of R6G. Obviously, SERS spectra of R6G became weak as decreasing R6G concentration. The characteristic Raman peaks of R6G at 1651 cm^{-1} was also found when the concentration of R6G is as low as 10^{-10} M. The average enhancement factors (EF) were estimated according to the formula $EF = (I_{SERS}/I_{Raman})/(N_{surface}/N_{bulk})$ in our early report.[5] I_{SERS} stands for the intensities of the vibrational mode in the SERS spectra and I_{Raman} stands for the same vibrational mode in the normal Raman spectra. These data can be directly obtained from the experiment. N_{bulk} and $N_{surface}$ are the number of R6G molecules illuminated by the laser focus spot under normal Raman and SERS conditions, respectively. In the normal Raman spectrum, the neat solid sample was obtained by dropping 10^{-2} M R6G aqueous on the glass and dried in air. The dissolved concentration of R6G was 10^{-7} M in the

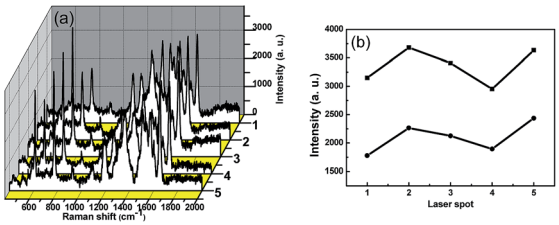

Fig. 6 (a) The SERS spectra of R6G (1×10^{-5} M) were obtained on different spots of TiO_2/Ag nanocomposites (b) corresponding Raman peak intensity at Raman shift of 1651 cm^{-1} and 769 cm^{-1}, respectively.

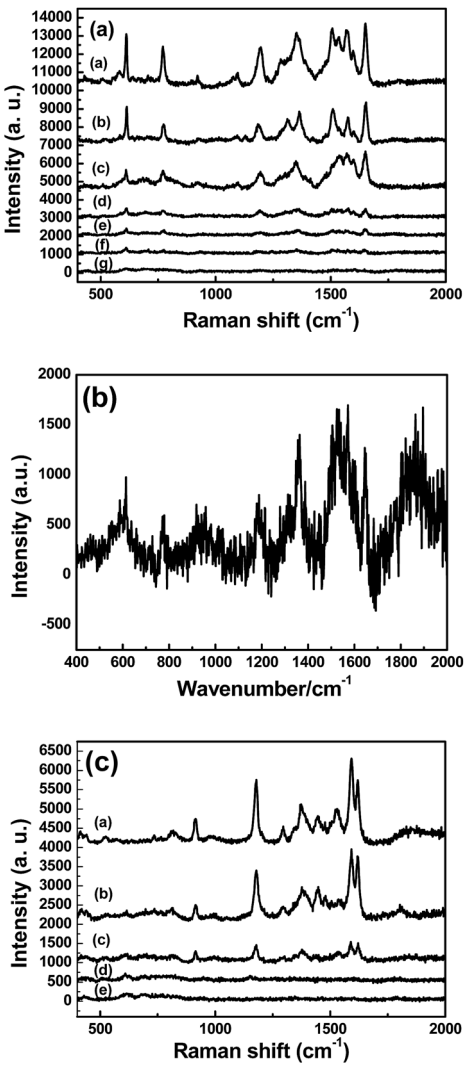

Fig. 7 (a) SERS spectra of different concentration of R6G absorbed on the TiO_2/Ag nanocomposites S_{r3} (curve a–g corresponding to 10^{-5}–10^{-11} M) (b) Raman spectrum R6G on commercial glass substrate (c) SERS spectra of different concentration of CV absorbed on the TiO_2/Ag nanocomposites S_{r3} (curve a–e corresponding to 10^{-5}–10^{-9} M).

SERS spectrum. Here we obtained that the I_{SERS} and I_{Raman} are 1908 (Fig. 7a) and 1231 (Fig. 7b) counts at the Raman band of 1651 cm^{-1}, respectively. The volumes of the irradiated laser spots in the Raman and SERS experiments were identical. The density of 1.15 g cm^3 for the solid R6G, the enhancement factor

may be estimated as, $(1908) \times (10^7) \times 1/(1231 \times (1.15/479) \times 10^3) = 6.46 \times 10^6$. The value of EF is determined to be in the order of 10^6. Crystal violet (CV) was also used to further the SRES sensitivity of S_{r3}. Fig. 7c shows the SERS spectra using S_{r3} substrate for different concentrations of CV. Typical Raman peaks of CV at 915 cm^{-1} (ring skeletal vibration of radial orientation), 1178 cm^{-1} (in plane ring C–H bending), 1295 cm^{-1} (ring C–C stretching) and 1531, 1592, 1619 cm^{-1} (ring C–C stretching) can be obviously observed.[51] It is clear that the characteristic SERS spectra at 1619 cm^{-1} of CV were also found when the concentration of CV decreased to 10^{-7} M. It can be concluded that the TiO_2/Ag nanocomposites substrate (S_{r3}) is highly sensitive and it is sufficient enough to directly observe a trace amount of organic dyes.

TiO_2 nanostructures have wide potential application as the renewable SERS substrate due to its high ability in the photocatalytic degradation. The SERS recyclable applications of TiO_2/Ag were examined. Following the irradiation time of 1 h, the substrate was again immersed in 10^{-5} M of dyes (R6G and CV) solution. Fig. 8 shows that the SERS signals are well reproduced after each UV-visible light cleaning and dyes adsorption (10^{-5} M). No Raman signal of R6G and CV molecules is detected anymore after 1 h irradiation of UV-visible light, suggesting that the dye molecules are degraded into small molecules such as CO_2 and H_2O. The dependence of SERS signals on the length of irradiation time in Fig. S2† further testified that S_{r3} could be as self-cleaning substrate materials.

Photocurrents for the as-synthesized samples were also measured on a Zahner workstation (Zahner, German) with a LW405 light (wavelength at 405 nm, 10 mW cm^{-2}) as the accessory light source to investigate the electronic interaction between Ag and TiO_2 (Fig. 9). All experiments were performed with a conventional three electrode system. A modified indium tin oxide (ITO) electrode (1×0.5 cm^2) was used as working electrodes. An Ag/AgCl (satd KCl) electrode and a Pt wire electrode were used as reference and counter electrodes, respectively. All the photocurrent responses were collected at open circuit potentials (see Fig. S3†). Under light irradiation, fast and uniform photocurrent responses were observed in all rutile TiO_2/Ag nanocomposites. It is clearly that the photocurrent density of the S_{r3} electrode was higher than that of the other samples in Fig. 9. The result means that S_{r3} can be induced to generate more electrons and holes under light irradiation, which will enhance the photocatalytic efficiency.

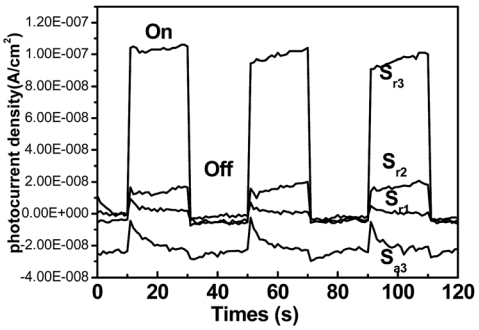

Fig. 9 Photocurrents of TiO_2/Ag nanocomposites electrodes under visible light irradiation.

The possible mechanism of the good SERS and photocatalytic performance of the TiO_2/Ag nanocomposite (S_{r3}) was also discussed. The SERS enhancement of TiO_2/Ag nanocomposite (S_{r3}) should be attributed to the combination of small size and the high content of Ag nanoparticles. On the one hand, the small size and high density of Ag nanoparticles, suitable for the generation of Raman "hot spots" is important for electromagnetic enhancement. For the substrates with relative few silver nanoparticles (S_{r1}, S_{r2} and S_a), the electromagnetic enhancement is relative weak. On the other hand, for photocatalytic performance of S_{r3}, electromagnetic effect also improve the photocatalytic efficiency.

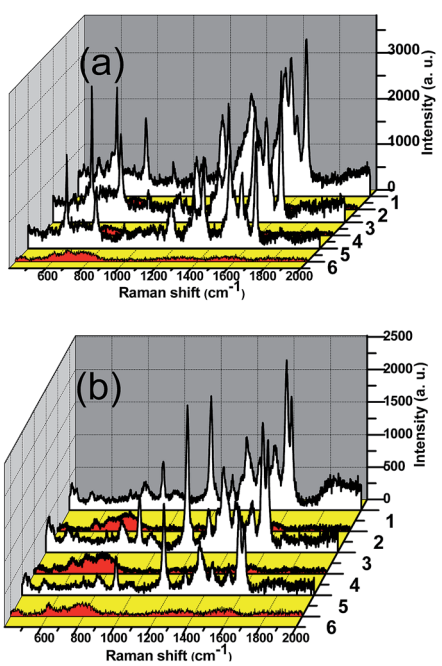

Fig. 8 SERS spectra of (a) R6G (10^{-5} M) and (b) CV (10^{-5} M) absorbed on the TiO_2/Ag nanocomposites and the repeating cleaning and recovery processes for three cycles (1,3,5-dyes absorption, 2,4,6-self cleaning after irradiation).

4. Conclusions

In conclusion, commercial anatase titanium oxide (TiO_2) and rutile titanium oxide (TiO_2) were used to prepare TiO_2/Ag nanocomposites by a simple photochemical method. Experiments testified rutile TiO_2/Ag nanocomposite (S_{r3}) to be a kind of excellent substrate for SERS detection of organic dyes. Meanwhile, target organic dyes can be degraded into clean inorganic molecules *in situ* by UV-visible irradiation on this substrate. The possible mechanism of the good SERS and photocatalytic performance of the TiO_2/Ag nanocomposite (S_{r3}) was discussed. This recyclable strategy opens a new opportunity in avoiding the single-use problem of traditional SERS substrates.

Acknowledgements

This work was financially supported by the National Natural Science Foundation of China (NSFC, No. 21505118), and the Natural Science Foundation of Jiangsu Province (No. BK20150438).

References

1 N. L. Gruenke, M. F. Cardinal, M. O. McAnally, R. R. Frontiera, G. C. Schatz and R. P. Van Duyne, *Chem. Soc. Rev.*, 2016, **45**, 2263–2290.
2 Y. Q. Zhu, L. Zhang and L. B. Yang, *Mater. Res. Bull.*, 2015, **63**, 199–204.
3 B. Sharma, R. R. Frontiera, A. I. Henry, E. Ringe and R. P. Van Duyne, *Mater. Today*, 2012, **15**, 16–25.
4 K. B. Zhang, T. X. Zen, X. L. Tan, W. D. Wu, Y. J. Tang and H. B. Zhang, *Appl. Surf. Sci.*, 2015, **347**, 569–573.
5 Q. L. Huang, J. M. Wang, W. X. Wei, Q. X. Yan, C. L. Wu and X. S. Zhu, *J. Hazard. Mater.*, 2015, **283**, 123–130.
6 X. Gong, Y. Bao, C. Qiu and C. Y. Jiang, *Chem. Commun.*, 2012, **48**, 7003–7018.
7 C. Feng, Y. Zhao and Y. J. Jiang, *RSC Adv.*, 2016, **6**, 83273–83279.
8 M. D. Thi and K. Volka, *J. Mol. Struct.*, 2010, **976**, 297–300.
9 P. H. Zhang, Y. M. Sui, C. Wang, Y. N. Wang, G. L. Cui, C. Z. Wang, B. B. Liu and B. Zou, *Nanoscale*, 2014, **6**, 5343–5350.
10 B. Luo, G. Liu and L. Z. Wang, *Nanoscale*, 2016, **8**, 6904–6920.
11 C. M. Li, Y. Xu, W. G. Tu, G. Chen and R. Xu, *Green Chem.*, 2017, **19**, 882–899.
12 M. Z. Ge, C. Y. Cao, J. Y. Huang, S. H. Li, Z. Chen, K.-Q. Zhang, S. S. Al-Deyab and Y. K. Lai, *J. Mater. Chem. A*, 2016, **4**, 6772–6801.
13 Y. F. Wang, L. P. Li, X. S. Huang, Q. Li and G. S. Li, *RSC Adv.*, 2015, **5**, 34302–34313.
14 X. He, H. Wang, Z. B. Li, D. Chen, J. H. Liu and Q. Zhang, *Nanoscale*, 2015, **7**, 8619–8626.
15 R. Li, C. Han and Q.-W. Chen, *RSC Adv.*, 2013, **3**, 11715–11722.
16 L. B. Yang, P. Li and J. H. Liu, *RSC Adv.*, 2014, **4**, 49635–49646.
17 L. H. Dong, J. Y. Zhu and G. Q. Xia, *Solid State Sci.*, 2014, **38**, 7–12.
18 Y. Sun, *Adv. Funct. Mater.*, 2010, **20**, 3646–3657.
19 S. Y. Cui, Z. G. Dai, Q. Y. Tian, J. Liu, X. H. Xiao, C. Z. Jiang, W. Wu and V. A. L. Roy, *J. Mater. Chem. C*, 2016, **4**, 6371–6379.
20 X. He, H. Wang, Z. B. Li, D. Chen and Q. Zhang, *Phys. Chem. Chem. Phys.*, 2014, **16**, 14706–14712.
21 K. Y. Zhao, J. Lin and L. Guo, *RSC Adv.*, 2015, **5**, 53524–53528.
22 X. B. Chen, L. Liu and F. G. Huang, *Chem. Soc. Rev.*, 2015, **44**, 1861–1885.
23 W. Wang, Y. Liu, J. F. Qu, Y. B. Chen and Z. P. Shao, *RSC Adv.*, 2016, **6**, 40923–40931.
24 X. F. Zhang, Y. N. Wang, B. S. Liu, Y. H. Sang and H. Liu, *Appl. Catal., B*, 2017, **202**, 620–641.
25 J. W. Wang, G. Q. Xu, X. Zhang, J. Lv, D. M. Wang, Z. X. Zheng, J. M. Wang and Y. C. Wu, *New J. Chem.*, 2015, **39**, 9019–9027.
26 Q. Guo, C. Y. Zhou, Z. B. Ma, Z. F. Ren, H. J. Fan and X. M. Yang, *Chem. Soc. Rev.*, 2016, **45**, 3701–3730.
27 Y. Y. Zhang, Z. L. Jiang, J. Y. Huang, L. Y. Lim, W. L. Li, J. Y. Deng, D. G. Gong, Y. X. Tang, Y. K. Lai and Z. Chen, *RSC Adv.*, 2015, **5**, 79479–79510.
28 L. Gomathi Devi and R. Kavitha, *Appl. Surf. Sci.*, 2016, **360**, 601–622.
29 X. Q. Liu, J. Iocozzia, Y. Wang, X. Cui, Y. H. Chen, S. Q. Zhao, Z. Li and Z. Q. Lin, *Energy Environ. Sci.*, 2017, **10**, 402–434.
30 L. Zhang, D. C. Shi, B. C. Liu, G. Zhang, Q. Wang and J. Zhang, *CrystEngComm*, 2016, **18**, 6444–6452.
31 Y. Zhang, T. Wang, M. Zhou, Y. Wang and Z. M. Zhang, *Ceram. Int.*, 2017, **43**, 3118–3126.
32 Y.-C. Yao, X.-R. Dai, X.-Y. Hu, S.-Z. Huang and Z. Jin, *Appl. Surf. Sci.*, 2016, **387**, 469–476.
33 M. X. Sun, Y. L. Fang, S. F. Sun and Y. Wang, *RSC Adv.*, 2016, **6**, 12272–12279.
34 S. S. Boxi and S. Paria, *RSC Adv.*, 2015, **5**, 37657–37668.
35 S. Yurdakal, B. S. Tek, Ç. Değirmenci and G. Palmisano, *Catal. Today*, 2017, **281**, 53–59.
36 H. Fang, C. X. Zhang, L. Liu, Y. M. Zhao and H. J. Xu, *Biosens. Bioelectron.*, 2015, **64**, 434–441.
37 X. L. Chong, B. Zhao, R. Li, W. D. Ruan and X. W. Yang, *Colloids Surf., A*, 2015, **481**, 7–12.
38 L. B. Yang, X. Jiang, W. D. Ruan, J. X. Yang, B. Zhao, W. Q. Xu and J. R. Lombardi, *J. Phys. Chem. C*, 2009, **113**, 16226–16231.
39 X. X. Zou, R. Silva, X. X. Huang, J. F. Al-Sharab and T. Asefa, *Chem. Commun.*, 2013, **49**, 382–384.
40 X. X. Xue, D. D. Xu, W. D. Ruan, L. Chen, L. M. Chang and B. Zhao, *RSC Adv.*, 2015, **5**, 64235–64239.
41 Y. F. Shan, Y. Yang, Y. Q. Cao, H. Yin, N. V. Long and Z. R. Huang, *RSC Adv.*, 2015, **5**, 34737–34743.
42 I. Tanahashi and Y. Harada, *J. Mater. Chem. C*, 2015, **3**, 5721–5726.
43 W. Zhou, B.-C. Yin and B.-C. Ye, *Biosens. Bioelectron.*, 2017, **87**, 187–194.
44 Z. Y. Zhang, J. J. Yu, J. Y. Yang, X. Lv and T. H. Wang, *Appl. Surf. Sci.*, 2015, **359**, 853–859.
45 Q. Q. Ding, L. Zhang and L. B. Yang, *Mater. Res. Bull.*, 2014, **53**, 205–210.
46 Z. Y. Bao, X. Liu, J. Y. Dai, Y. C. Wu, Y. H. Tsang and D. Y. Lei, *Appl. Surf. Sci.*, 2014, **301**, 351–357.
47 Y. B. Xie, Y. Y. Jin, Y. Z. Zhou and Y. Wang, *Appl. Surf. Sci.*, 2014, **313**, 549–557.
48 X. Fu, L. J. Pan, S. Li, Q. Wang, J. Qin and Y. Y. Huang, *Appl. Surf. Sci.*, 2016, **363**, 412–420.
49 X. H. Li, G. Chen, L. Yang, Z. Jin and J. Liu, *Adv. Funct. Mater.*, 2012, **20**, 2815–2824.
50 X. J. Wang, W. Y. Yang, F. T. Li, Y. B. Xue, R. H. Liu and Y. J. Hao, *Ind. Eng. Chem. Res.*, 2013, **52**, 17140–17150.
51 W. X. Wei and Q. L. Huang, *Spectrochim. Acta, Part A*, 2017, **179**, 211–215.